Investigation Into Multi-Layer Fractional-Slot Concentrated Windings With Unconventional Slot-Pole Combinations

Alberto Tessarolo, *Senior Member, IEEE*, Cesare Ciriani, Mauro Bortolozzi, Mario Mezzarobba, and Nicola Barbini

***Abstract*—Fractional-slot concentrated windings (FSCWs) are an attractive option for the design of synchronous permanent-magnet machines. It is commonly assumed in the existing literature that a symmetrical three-phase FSCW is feasible only on a condition that the number of slots Z is an integer multiple of three times the maximum common divisor between Z and the number of pole pairs p. Slot-pole combinations satisfying this rule can be defined conventionally, the others unconventionally. In contrast to the common belief, this paper shows that, using a multi-layer arrangement, it is possible to synthetize a symmetrical FSCW having unconventional slot-pole combinations. A general design methodology for this purpose is presented and validated by finite element analysis. The pros and contras of FSCWs with unconventional slot-pole combinations are examined. Finally, the application of an unconventional FSCW to a shipboard surface permanent-magnet machine prototype is presented to illustrate the possible practical convenience of this kind of winding and tests on the prototype are reported for experimental validation.**

***Index Terms*—Concentrated winding, design optimization, fractional slot, permanent-magnet machines, quadratic programming, slot-pole combinations.**

I. Introduction

FRACTIONAL-SLOT concentrated winding (FSCW) is gaining increasing popularity for electric machine stator construction as it is easy to manufacture, gives short end coils, helps reduce resistive losses, allows for modular architectures and better flux weakening performance [1]. Among the various types of FSCW variants, the dual-layer one (with a single coil wound on each tooth) is the most frequent choice [2]. It is commonly assumed in the literature [3] that, for a three-phase dual-layer FSCW with Z slots and p pole pairs to be symmetrical, the number of slots Z must be and integer multiple of $3K$, being K the maximum common divisor between the number of slots Z and the number of pole pairs p: such rule is commonly presented as a general condition for the winding feasibility even if multi-layer design solutions are used [2]. Slot-pole combinations satisfying the rule are hereinafter referred to as conventional, while the others are defined unconventional.

The way how the number of slots and poles is chosen strongly affects machine performance in various respects, such as: winding factor [4], [5], radial forces and vibration behavior [6]–[8], cogging torque [9], [10], flux-weakening capability [11] and leakage inductances [12]. Therefore, the need to choose the number of slots and poles, Z and $2p$, among conventional slot-pole combinations poses a limitation to the designer as it narrows the scope of the design solutions for machine performance optimization.

The idea of broadening the range of feasible slot-pole combinations beyond the currently assumed limits is suggested by a recent work [13], which demonstrates how a quasi-symmetrical 39-slot 12-pole winding can be designed with good performance. However, the treatment in [13] lacks generality as it applies to winding layouts composed of three-slot pitch coils.

The goal of this paper is to prove that, contrary to the common belief, a perfectly symmetrical FSCW can be obtained even with unconventional pole-slot combinations, on condition that a multi-layer winding arrangement (with one or two coils per tooth) is used [2], [14]–[18]. A design methodology to synthetize FSCWs with unconventional slot-pole combinations, based on the quadratic-programming approach proposed in [16], is first presented and validated through finite-element analysis (FEA) simulations. Conventional and unconventional slot-pole combinations are then compared in terms of winding factor, rotor eddy-current losses, torque ripple and radial forces. Overall, it is shown that unconventional FSCW's have very variable performance depending on the slot-pole combination just like conventional ones. Thereby, they cannot be claimed to outperform the traditional design in general. Rather, the key finding is that unconventional FSCW's are feasible and can be synthetized with a well-defined algorithm. This extends the range of possible winding layouts, leading to new solutions which may fit specific applications more than conventional slot-pole combinations. As

Manuscript accepted July 15, 2019.. This work was supported by Regione Autonoma Friuli Venezia Giulia, Italy, under POR-FESR 2014-2020 Funding Program. Paper no. TEC-00011- 2019. (*Corresponding author: Alberto Tessarolo*.)

A. Tessarolo, C. Ciriani, M. Mezzarobba, and N. Barbini are with Engineering and Architecture Department, University of Trieste, 34127 Trieste, Italy (e-mail: atessarolo@units.it; cesare.ciriani@phd.units.it; mmezzarobba@units.it; nicola.barbini@phd.units.it).

M. Bortolozzi is with Rete Ferroviaria Italiana, 34145 Trieste, Italy (e-mail: m.bortolozzi@rfi.it).

TABLE I
DEFINITION OF THE k-TH TOOTH VECTOR ELEMENTS

Vector element	Meaning
$[\mathbf{x}_{\text{tooth},k}]_0$	Number of phase-*a* turns wound on tooth k in CW. sense
$[\mathbf{x}_{\text{tooth},k}]_1$	Number of phase-*c* turns wound on tooth k in CCW sense
$[\mathbf{x}_{\text{tooth},k}]_2$	Number of phase-*b* turns wound on tooth k in CW sense
$[\mathbf{x}_{\text{tooth},k}]_3$	Number of phase-*a* turns wound on tooth k in CCW sense
$[\mathbf{x}_{\text{tooth},k}]_4$	Number of phase-*c* turns wound on tooth k in CW sense
$[\mathbf{x}_{\text{tooth},k}]_5$	Number of phase-*b* turns wound on tooth k in CCW sense

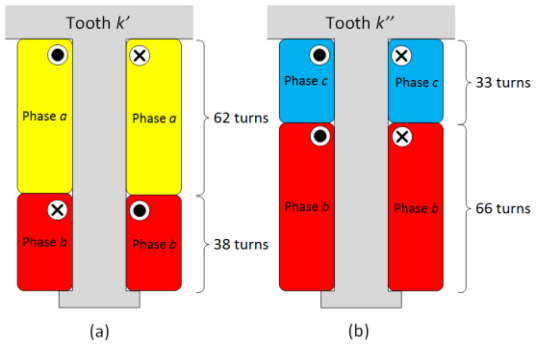

Fig. 1. Examples of tooth windings for (a) the k'-th tooth; (b) the k''-th tooth. Symbols ⊙ and ⊗ indicate the conventional current direction.

an example and case study, the application of an unconventional FSCW to an SPM shipboard generator prototype is discussed and some test results on it are reported for experimental validation.

II. DESIGN METHODOLOGY FOR A MULTI-LAYER FSCW WITH A GENERIC SLOT-POLE COMBINATION

In [16] a quadratic-programming approach is presented for the design optimization of a FSCW with reduced rotor losses. In this Section, the approach is briefly recalled and then adapted to the purpose of designing a three-phase FSCW with a generic number of slots Z and pole pairs p.

A. Symmetric FSCW Modeling

In order to define the design algorithm, it is necessary to mathematically describe the structure of the generic FSCW which includes Z wound teeth. To this end, the Z teeth are numbered sequentially with an index k ranging from 0 to $Z-1$. The winding of the generic k^{th} tooth is characterized by a 6-sized positive-defined tooth vector $\mathbf{x}_{\text{tooth},k}$. The six elements of the vector are defined as explained in Table I, where the clockwise (CW) and counter-clockwise (CCW) senses refer to the direction in which a turn is wound around the tooth, if viewed from the air-gap.

For example, the tooth windings shown in Fig. 1(a) and Fig. 1(b) and referring to the k'-th and k''-th tooth, are characterized by the following tooth vectors:

$$\mathbf{x}_{\text{tooth},k'} = \begin{pmatrix} 0 & 0 & 38 & 62 & 0 & 0 \end{pmatrix}^T, \tag{1}$$

$$\mathbf{x}_{\text{tooth},k''} = \begin{pmatrix} 0 & 33 & 0 & 0 & 0 & 66 \end{pmatrix}^T, \tag{2}$$

where superscript T denotes transposition.

Calling N_{tooth} the maximum number of turns that can be wound around each tooth (100 in case of Fig. 1), the following constraint must obviously hold for any k:

$$\sum_{n=0..5} [\mathbf{x}_{\text{tooth},k}]_n \le N_{\text{tooth}}. \tag{3}$$

The whole winding can be characterized by the $6Z$-sized winding vector $\mathbf{x}$ obtained by stacking all the tooth vectors:

$$\mathbf{x} = \begin{pmatrix} \mathbf{x}_{\text{tooth},0} \\ \mathbf{x}_{\text{tooth},1} \\ \vdots \\ \mathbf{x}_{\text{tooth},Z-1} \end{pmatrix}. \tag{4}$$

Based on (3), the winding vector $\mathbf{x}$ is subject to the following matrix inequality constraint:

$$\mathbf{A}_{\text{in}}\mathbf{x} \le \mathbf{b}_{\text{in}}, \tag{5}$$

where $\mathbf{A}_{\text{in}}$ is the $Z \times 6Z$ matrix and $\mathbf{b}_{\text{in}}$ is the $6Z$ vector below:

$$\mathbf{A}_{\text{in}} = \begin{pmatrix} \mathbf{1}_{1\times6} & \mathbf{0}_{1\times6} & \cdots & \mathbf{0}_{1\times6} \\ \mathbf{0}_{1\times6} & \mathbf{1}_{1\times6} & \cdots & \mathbf{0}_{1\times6} \\ \vdots & \vdots & \ddots & \vdots \\ \mathbf{0}_{1\times6} & \mathbf{0}_{1\times6} & \cdots & \mathbf{1}_{1\times6} \end{pmatrix}, \mathbf{b}_{\text{in}} = N_{\text{tooth}}\mathbf{1}_{Z\times1} \tag{6}$$

being $\mathbf{1}_{m,n}$ and $\mathbf{0}_{m,n}$ the $m \times n$ matrices having all their entries respectively equal to 1 and 0.

As a result demonstrated in [16] we know that, if the three phases carry the symmetrical balanced current system of amplitude I_0 and angular frequency ω:

$$\begin{aligned} &i_a(t) = I_0 \cos(\omega t), i_b(t) = I_0 \cos\left(\omega t - \tfrac{2}{3}\pi\right), \\ &i_c(t) = I_0 \cos\left(\omega t - \tfrac{4}{3}\pi\right), \end{aligned} \tag{7}$$

then the FSCW produces an air-gap MMF fundamental of amplitude M_{fund} such that its square can be expressed as a quadratic function of the winding vector $\mathbf{x}$:

$$M_{\text{fund}}{}^2 = \mathbf{x}^T \mathbf{Q}\, \mathbf{x}, \tag{8}$$

where $\mathbf{Q}$ is a $6Z \times 6Z$ real symmetric matrix. As proved in [16], $\mathbf{Q}$ is given by:

$$\mathbf{Q} = \mathbf{c}\,\mathbf{c}^T + \mathbf{s}\,\mathbf{s}^T, \tag{9}$$

where $\mathbf{c}$ and $\mathbf{s}$ are the $6Z$-sized column vectors defined as:

$$\begin{aligned} [\mathbf{s}]_n &= \frac{(-1)^p}{p\pi} \sin\left(\frac{\pi\, p\,(Z-1)}{Z}\right) \\ &\quad \times I_0 \sin\left[p\tfrac{2\pi}{Z}\text{floor}\left(\frac{n}{6}\right) - \tfrac{\pi}{3} \bmod (n,6)\right] \\ [\mathbf{c}]_n &= \frac{(-1)^p}{p\pi} \sin\left(\frac{\pi\, p\,(Z-1)}{Z}\right) \\ &\quad \times I_0 \cos\left[p\tfrac{2\pi}{Z}\text{floor}\left(\frac{n}{6}\right) - \tfrac{\pi}{3} \bmod (n,6)\right] \end{aligned} \tag{10}$$

for any n between 0 and $6Z-1$ and with functions floor(x) and mod(x, y) respectively returning the integer part of x and the remainder on dividing x by y.

Finally, it is demonstrated in [16] that the electrical symmetry of the FSCW imposes the following matrix equality constraint on the winding vector:

$$\mathbf{A}_{\mathrm{eq}}\mathbf{x} = \mathbf{b}_{\mathrm{eq}}, \tag{11}$$

where $\mathbf{A}_{\mathrm{eq}}$ is the $4 \times 6Z$ matrix and $\mathbf{b}_{\mathrm{eq}}$ is the vector below:

$$\mathbf{A}_{\mathrm{eq}} = \begin{pmatrix} \mathbf{c}^T(\mathbf{K}_b - \mathbf{K}_a) \\ \mathbf{s}^T(\mathbf{K}_b - \mathbf{K}_a) \\ \mathbf{c}^T(\mathbf{K}_c - \mathbf{K}_b) \\ \mathbf{s}^T(\mathbf{K}_c - \mathbf{K}_b) \end{pmatrix}, \quad \mathbf{b}_{\mathrm{eq}} = \begin{pmatrix} 0 \\ 0 \\ 0 \\ 0 \end{pmatrix}, \tag{12}$$

with $\mathbf{c}$ and $\mathbf{s}$ given by (10) and $\mathbf{K}_a$, $\mathbf{K}_b$, $\mathbf{K}_c$ being $6Z \times 6Z$ diagonal matrices defined as follows:

$$[\mathbf{K}_a]_{m,n} = \begin{cases} 1 & \text{if } m = n \text{ and } \mathrm{mod}(m,\ 3) = 0 \\ 0 & \text{otherwise} \end{cases},$$

$$[\mathbf{K}_b]_{m,n} = \begin{cases} 1 & \text{if } m = n \text{ and } \mathrm{mod}(m,\ 3) = 1 \\ 0 & \text{otherwise} \end{cases},$$

$$[\mathbf{K}_c]_{m,n} = \begin{cases} 1 & \text{if } m = n \text{ and } \mathrm{mod}(m,\ 3) = 2 \\ 0 & \text{otherwise} \end{cases}, \tag{13}$$

for any m and n ranging from 0 to $6Z - 1$.

B. FSCW Design Algorithm Formulation

Based on the mathematical relationships recalled in the previous subsection, the problem of designing a symmetric FSCW with Z slots and p pole pairs can be formulated in terms of determining a winding vector $\mathbf{x}$ that maximizes the air-gap MMF fundamental amplitude [hence its square (8)] while satisfying constraints (6) and (11). The objective of maximizing the MMF fundamental is obviously justified by the need to obtain a FSCW layout with the highest possible winding factor. The FSCW design is thus reduced to the solution of the following quadratic programming problem:

$$\begin{aligned} &\text{maximize } \mathbf{x}^T\mathbf{Q}\,\mathbf{x} \\ &\text{subject to } \mathbf{A}_{\mathrm{in}}\mathbf{x} \le \mathbf{b}_{\mathrm{in}},\ \mathbf{A}_{\mathrm{eq}}\mathbf{x} = \mathbf{b}_{\mathrm{eq}},\ \mathbf{x} \ge 0. \end{aligned} \tag{14}$$

The formulation (14) differs from that considered in [16] because it is a single-objective problem, which can be straightforwardly solved in the Matlab environment. As a solution of (14), the optimal winding vector is obtained, and, from this, it is possible to fully determine the whole winding layout. To this end, it is sufficient to extract the Z tooth winding vectors according to (4): the six elements of k^{th} winding vector indicate (according to Table I) how many turns are to be wound on the k^{th} tooth for any phase, and in which sense.

It may be worth noting that all the matrices $\mathbf{Q}$, $\mathbf{A}_{\mathrm{eq}}$, $\mathbf{b}_{\mathrm{eq}}$, $\mathbf{A}_{\mathrm{in}}$ and $\mathbf{b}_{\mathrm{in}}$ appearing in (14) do not depend on the machine geometry, as proved by their analytical formulations recalled in Section II-A. Hence, the FSCW layout obtained from the solution of (14) is the same irrespective of machine geometry and dimensions.

It is important to observe that, in both deriving and using the equations reported in the previous subsection, no restrictive hypothesis has been made on Z and p, which can be two arbitrary integers. This suggests that the optimization problem (14) may yield a solution even for those slot-pole combinations which are commonly regarded as unsuitable for a symmetric winding design. This fact will be confirmed in the next Section focusing on two case studies (8-slot 6-pole and 11-slot 10-pole FSCWs).

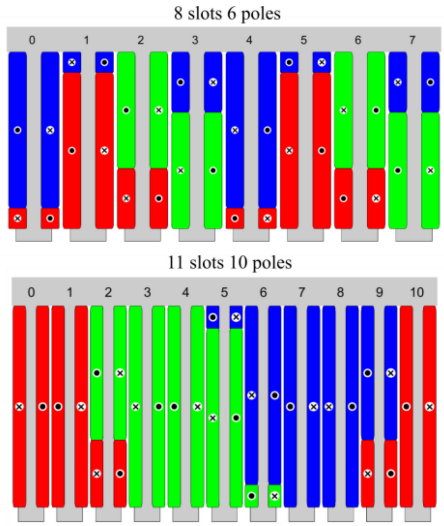

Fig. 2. Winding layouts for a FSCW with 8 slots and 6 poles and with 11 slots and 10 poles.

TABLE II
TURNS PER TOOTH PER PHASE IN THE 8-SLOT 6-POLE WINDING

	Tooth index							
	k=0	k=1	k=2	k=3	k=4	k=5	k=6	k=7
Phase $+a$	11	0	30	0	0	77	0	0
Phase $-a$	0	77	0	0	11	0	30	0
Phase $+b$	0	0	0	58	0	0	58	0
Phase $-b$	0	0	58	0	0	0	0	58
Phase $+c$	0	11	0	0	77	0	0	30
Phase $-c$	77	0	0	30	0	11	0	0

III. DESIGN AND PERFORMANCE ASSESSMENT OF AN 8-SLOT 6-POLE AND OF AN 11-SLOT 10-POLE FSCW

For illustration purposes, the problem (14) is herein solved for two example slot-pole combinations, which are: $Z = 8$, $2p = 6$ and $Z = 11$ and $2p = 10$. For the 8-slot 6-pole winding the maximum number N_{tooth} of turns which can be wound around a tooth is set to 88, while for the 11-slot 10-pole machine it is assumed equal to 100.

The FSCW layouts, which result from the numerical solution of (7) in the two cases, are shown in Fig. 2 and the numbers of turns per tooth per phase are detailed in Table II and Table III.

For the sake of simplicity, in Table II and Table III as well as in the rest of the paper, each phase is designed with sign "+" if wound in CW sense and sign "–" otherwise.

In order to assess the performance of the two synthetized windings, they are applied to a sample SPM machine and compared to a couple of similar conventional winding configuration, having the same pole count: the 8-slot 6-pole winding

TABLE III
TURNS PER TOOTH PER PHASE IN THE 11-SLOT 10-POLE WINDING

	Tooth index										
	k=0	k=1	k=2	k=3	k=4	k=5	k=6	k=7	k=8	k=9	k=10
Phase $+a$	100	0	33	0	0	0	0	0	0	33	0
Phase $-a$	0	100	0	0	0	0	0	0	0	0	100
Phase $+b$	0	0	0	100	0	89	0	0	0	0	0
Phase $-b$	0	0	67	0	100	0	11	0	0	0	0
Phase $+c$	0	0	0	0	0	0	89	0	100	0	0
Phase $-c$	0	0	0	0	0	11	0	100	0	67	0

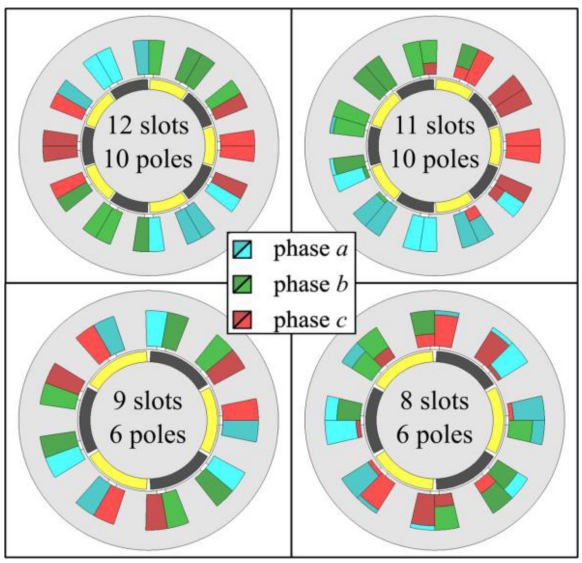

Fig. 3. Cross sections of the four SPM machines considered for performance comparison.

TABLE IV
DESIGN DATA OF THE SPM MACHINES UNDER COMPARISON

	9 slots 6 poles	8 slots 6 poles	12 slots 10 poles	11 slots 10 poles
Nr. of turns per tooth, N_{tooth}	100	100	100	100
Phase peak current, I_0	15.4 A	17.8 A	29.7 A	32.2 A
Magnet to pole span ratio	0.95	0.95	0.95	0.95
Magnet relative permeability	1.04	1.04	1.04	1.04
Magnet electrical conductivity	0.6 MS/m	0.67 MS/m	0.67 MS/m	0.67 MS/m
Magnet coercive force	800 kA/m	800 kA/m	800 kA/m	800 kA/m
Core relative permeability	10^5	10^5	10^5	10^5
Stator bore radius	60 mm	60 mm	100 mm	100 mm
Rotor core radius	49.5 mm	49.5 mm	82.5 mm	82.5 mm
Magnet height	9 mm	9 mm	15 mm	15 mm
Air gap width	1.5 mm	1.5 mm	2.5 mm	2.5 mm
Core length	100 mm	100 mm	100 mm	100 mm

is compared to the usual 9-pole 6-phase one and the 11-slot 10-pole winding is compared to the usual 12-slot 10-pole one. The cross sections of the SPM machines under comparison are shown in Fig. 3 and their characteristic design data are provided in Table IV. For the comparison to be fair, the same slot fill factor, conductor current density and magnetic loading [19] are applied to the all the four machines.

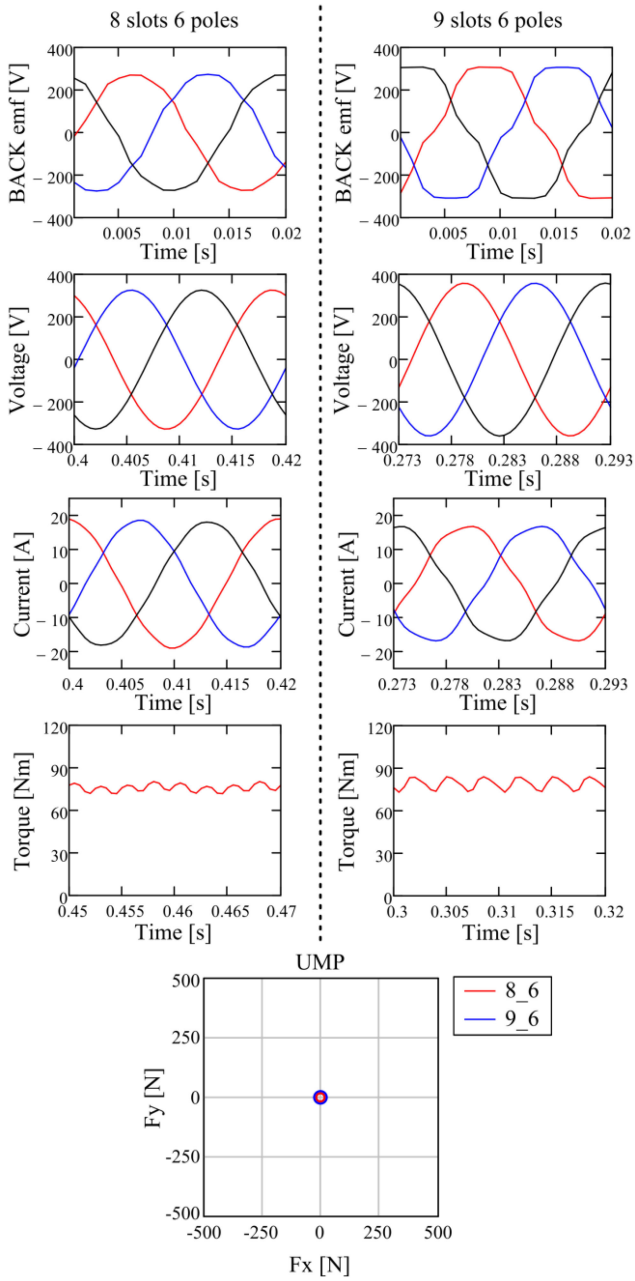

Fig. 4. Time-stepping FEA simulation results for the 9-slot 6-pole (conventional) and the 8-slot 6-pole (unconventional) machines working in their rated conditions.

To compare their performance, the four machines are modelled in the JMAG environment and a FEA time-stepping simulations are run with a sinusoidal 50 Hz voltage supply in the maximum-torque operating condition, in which the rated current (Table IV) is applied along the rotor q (inter-polar) axis [20].

Simulation results for the 6 pole machines are given in Fig. 4 and those for the 10 pole machines in Fig. 5. The considered diagrams show phase back Electro-Motive Forces (EMFs), supply voltages and currents, electromagnetic torque and radial force components (F_x and F_y) along two orthogonal (x and y) axes. The magnet losses resulting from simulations as well as from the

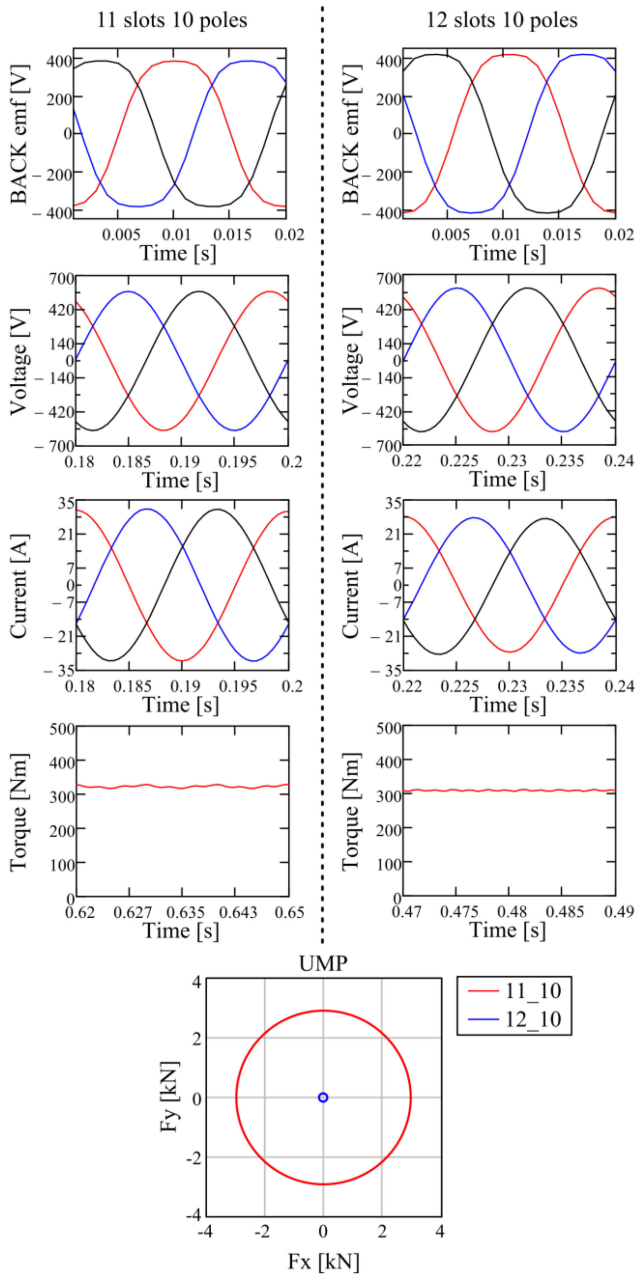

Fig. 5. Time-stepping FEA simulation results for the 12-slot 10-pole (conventional) and the 11-slot 10-pole (unconventional) machines working in their rated conditions.

analytical computation method described in [16] are reported in Table V.

Simulation results confirm that the synthetized unconventional FSCWs are perfectly symmetrical (as it can be seen from the back-EMF waveforms) and do not exhibit any kind of current imbalance when supplied from a sinusoidal three-phase source.

More particularly, the performance comparison for the 6-pole machines (Fig. 4) clearly shows that the unconventional FSCW produces a better EMF, which results in a less distorted stator current and a smaller torque ripple. Conversely, the mean torque is slightly higher for the conventional motor, since the 9-slot

TABLE V
PERMANENT MAGNET LOSS DENSITY FROM FEA AND ANALYSIS

	9 slots 6 poles	8 slots 6 poles	12 slots 10 poles	11 slots 10 poles
Magnet losses from FEA (W/mm^3)	0.16	0.25	0.57	0.67
Analytically computed magnet losses [16] (W/mm^3)	0.16	0.26	0.58	0.69

6-pole FSCW has a higher winding factor (0.866) than that (0.844) of the 8-slot 6-pole FSCW, as it will be discussed in Section IV. Regarding the radial forces, both winding configurations give a practically negligible Unbalanced Magnetic Pull (UMP). Finally, with respect to the magnet eddy-current losses (Table V), these are lower in the conventional machine, indicating a worse air gap MMF space harmonic spectrum from this standpoint.

Moving to the comparison between the 10-pole machines (Fig. 5), we can observe very similar performance in terms of EMF, current and torque harmonics. The unconventional configuration, however, suffers from higher permanent-magnet losses and a noticeably larger UMP compared to the conventional 12-slot 10-pole layout.

It is apparent from the mentioned case studies that unconventional designs cannot be said to give better or worse performance, in general. This justifies the interest of extending the comparison to a wider variety of slot-pole combinations, as done in the next Section.

IV. EXTENDED COMPARISON BETWEEN CONVENTIONAL AND UNCONVENTIONAL SLOT-POLE COMBINATIONS

The aim of this Section is to investigate the performance of FSCWs for a wide variety of both conventional and unconventional slot-pole combinations. The number of slots Z is assumed to vary in the range between 3 and 18, while the number of poles $2p$ between 2 and 24. A generic combinations of Z slots and $2p$ poles is conventional if

$$\frac{Z}{3 \times \mathrm{GCD}(Z,p)} \in \mathbb{Z}, \tag{15}$$

where $\mathbb{Z}$ is the set of integers, and unconventional otherwise. The number q of slots per phase is, in any case, defined as:

$$q = \frac{Z}{6p}. \tag{16}$$

For the purpose of the investigation, FSCWs with conventional slot-pole combinations are designed in their usual dual-layer form with the well-known star-of-slot method [2]. Conversely, FSCWs with unconventional slot-pole combinations are synthetized as discussed in Section II and exemplified in Section III, by solving the constrained quadratic programming problem (14).

However, it is noted that also conventional FSCWs can be, equivalently, designed by solving (14). In fact, taking the MMF fundamental maximization as the only objective function, (14) always yields the same optimal solution as the star-of-slot

TABLE VI
WINDING FACTOR FOR VARIOUS SLOT POLE COMBINATIONS. SHADED CELLS REPRESENT UNCONVENTIONAL COMBINATIONS

Number of slots \ Number of poles	2	4	6	8	10	12	14	16	18	20	22	24
3	0.866	0.866										
4	0.549		0.549									
5	0.546	0.883	0.883									
6		0.866		0.866								
7		0.736	0.918	0.918	0.736							
8		0.549	0.844		0.844							
9			0.866	0.945	0.945	0.866						
10			0.751	0.883		0.883	0.751					
11			0.718	0.864	0.940	0.940	0.864					
12				0.866	0.933		0.933	0.866				
13				0.783	0.889	0.944	0.944	0.889	0.783			
14				0.736	0.848	0.918		0.918	0.848			
15					0.866	0.883	0.951	0.951	0.883	0.866		
16					0.785	0.844	0.926		0.926	0.844	0.785	
17					0.760	0.853	0.916	0.949	0.949	0.916	0.853	
18						0.866	0.902	0.945		0.945	0.902	0.866

method when Z and p satisfy (15). This was already observed in [16] for 9-slot 8-pole machines and is confirmed for all the other slot-pole combinations investigated next.

As a further remark, it is noted that, in any case, (14) provides an optimal solution in which the constraint (3) is satisfied in its equality form, i.e., such that each tooth is wound with the maximum possible number of turns N_{tooth}.

Next, conventional and unconventional FSCW designs will be compared in terms of various performance or goodness indices, starting with the winding factor.

A. Winding Factor

Once the optimal winding vector x is obtained solving (14) for either a conventional or unconventional slot-pole combination, the winding factor k_{w} of the corresponding FSCW can be easily computed based on the well-known relationship [21]:

$$M_{\mathrm{fund}} = \frac{3}{\pi}\frac{k_{\mathrm{w}}}{p} N_{\mathrm{s}} I_0, \tag{17}$$

where: M_{fund} is the stator MMF fundamental amplitude, I_0 is the stator phase peak current and N_{s} is the number of series-connected turns per phase. By using (8) for M_{fund} and assuming the number of turns is series per phase given by:

$$N_{\mathrm{s}} = \frac{Z\, N_{\mathrm{tooth}}}{3}, \tag{18}$$

we obtain the following winding factor expression from (17):

$$k_{\mathrm{w}} = \frac{\pi p}{Z\, I_0\, N_{\mathrm{tooth}}} M_{\mathrm{fund}} = \frac{\pi\, p}{Z I_0\, N_{\mathrm{tooth}}} \sqrt{\mathbf{x}^T \mathbf{Q}\, \mathbf{x}}. \tag{19}$$

By means of (19) the winding factor is computed for all the slot-pole combinations with ¼ < q < ½, as these are the only ones which lead to acceptable winding factor values [8]. Results are reported in Table VI.

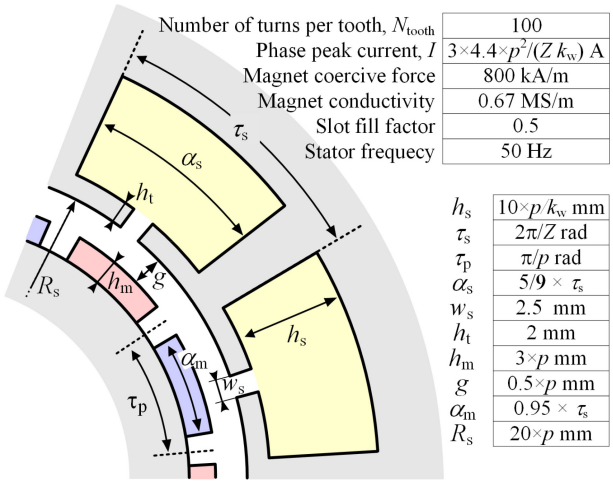

Fig. 6. Machine model for magnet eddy-current loss and UMP evaluation.

For conventional slot-pole combinations, the winding factors shown in Table VI and computed through (19) are exactly the same as those known from existing literature [8].

It can be seen from Table VI that the winding factor values are substantially consistent for conventional and unconventional slot-pole combinations. In both cases, k_{w} exhibits the same distribution, with similar top values all reached for winding configurations having Z $\cong$ 2p.

B. Rotor Eddy-Current Losses Due to MMF Harmonics

A further performance index for a FSCW is its content in MMF harmonics causing large eddy-current losses in the rotor conductive parts [22]. To investigate how this features varies with the chosen conventional or unconventional slot-pole combination, a homogenous comparison needs to be made between reasonably designed machines. For this purpose, the SPM machine model shown in Fig. 6 is considered for any number of slots Z and pole pair p.

By selecting machine parameters as indicated in Fig. 6, the conductor current density is maintained invariant (equal to 4 A/mm^2) as well as the air gap field due to both permanent magnets and armature reaction (as discussed in the Appendix), while machine dimensions keep realistic for any choice of Z = 3, 4, …, 18 and p = 1, 2, …, 12. Core length is not significant because magnet specific losses (per unit of volume) are considered. Results are reported in Table VII in terms of mW per magnet cube millimetre. The dependency of permanent-magnet eddy-current loss density on machine dimensions is investigated in [23] through a general approach which is fully applicable to both conventional and unconventional slot-pole combinations.

The losses in Table VII are computed through the analytical model described in [16] and results are cross-checked by independent time-stepping FEA simulations showing a maximum error below 5%.

As already observed for the winding factor, also magnet loss distribution and amplitudes appear from Table VII substantially

TABLE VII
MAGNET SPECIFIC LOSSES FOR VARIOUS SLOT POLE COMBINATIONS. SHADED CELLS ARE FOR UNCONVENTIONAL COMBINATIONS

Number of slots \ Numbers of poles	2	4	6	8	10	12	14	16	18	20	22	24
3	0.18	7.81										
4	0.07		20.63									
5	0.04	0.36	3.42									
6		0.17		7.73								
7		0.11	0.55	2.47	13.81							
8		0.06	0.26		4.58							
9			0.16	0.79	2.17	7.60						
10			0.11	0.33		3.30	11.48					
11			0.13	0.24	0.69	1.79	5.46					
12				0.15	0.58		2.88	7.51				
13				0.12	0.34	0.72	1.64	4.04	10.61			
14				0.09	0.19	0.49		2.35	5.71			
15					0.14	0.29	0.79	1.56	3.12	7.41		
16					0.11	0.22	0.53		2.02	4.28	9.64	
17					0.13	0.18	0.45	0.74	1.39	2.82	6.04	
18						0.13	0.38	0.72		2.01	3.67	7.19

TABLE VIII
PARAMETER C_{T} FOR VARIOUS SLOT-POLE COMBINATIONS. SHADED CELLS REPRESENT UNCONVENTIONAL COMBINATIONS

Number of slots \ Numbers of poles	2	4	6	8	10	12	14	16	18	20	22	24
3	1	1	3									
4	2		2									
5	1	1	1									
6		2		2								
7		1	1	1	1							
8		4	2		2							
9			3	1	1	3						
10			2	2		2	2					
11			1	1	1	1	1					
12				4	2		2	4				
13				1	1	1	1	1	1			
14				2	2	2		2	2			
15					5	3	1	1	3	5		
16					2	4	2		2	4	2	
17					1	1	1	1	1	1	1	
18						6	2	2		2	2	6

consistent for conventional and unconventional slot-pole combinations. This indicates that the MMF space harmonic content responsible for rotor eddy current losses cannot be, in general, said to be better for either conventional or unconventional FSCW designs.

C. Cogging Torque

The cogging torque in SPM machines is known to be independent of the winding layout. However, it strongly depends on the slot-pole combination, as well as on other design features like the slot opening width, the magnet to pole span ratio and the stator or rotor skewing [9].

With special regard to the slot-pole combination, [10] formally proves how the cogging torque is proportional to the following parameter:

$$C_{\mathrm{T}} = \frac{Z \times 2p}{\mathrm{LCM}(Z, 2p)}. \tag{20}$$

where LCM(x, y) is the least common multiple of x and y. Slot-pole combinations characterized by a large C_{T} are unfavourable in terms of cogging torque, while those having $C_{\mathrm{T}} = 1$ (the lowest possible value for C_{T}) are preferred.

Table VIII reports the values of C_{T} for various slot-pole combinations. The table shows that many unconventional combinations have $C_{\mathrm{T}} = 1$ and are therefore good possible candidates for the design of low-cogging-torque machines. In particular, all combinations where Z is an odd number not multiple of 3 (e.g., $Z = 5$, 7, 11, 13, etc.) enjoy the property of having $C_{\mathrm{T}} = 1$.

D. Radial forces

Radial forces arise in FSCW machines, even in absence of rotor eccentricity, each time the air gap magnetic field has a diametrically-asymmetrical distribution [24]. Conversely, the UMP is zero if the machine includes a sequence of repeatable groups of coils and poles [4], such that the radial forces generated by all groups have zero sum for symmetry reasons [25]. For example, it is well-known that 9-slot 8-pole combination suffers from high UMP [24]. The same has been observed for the 11-slot 10-pole machine considered in Section III: in fact, its winding lacks rotational symmetry as it can be seen from Fig. 3. On the other side, negligible UPM has been found in Section III for the 12-slot 10-pole, 8-slot 6-pole and 9-slot 6-pole combinations, which all enjoy a rotationally-symmetric winding layout (Fig. 3).

For a comprehensive comparison, the UMP is calculated considering various (conventional and unconventional) slot-pole combinations. For each of them, the machine model shown in Fig. 6 is built and studied by time-stepping FEA simulating its steady-state operation at rated current in the maximum-torque working point (i.e., with the armature reaction fundamental aligned to the q axis). The specific UMP is then obtained in terms of maximum radial force acting on a cm^2 of stator inner surface. Such a specific UMP constitutes a good index for homogeneously comparing different slot-pole combinations as explained in the Appendix. The specific UMP values obtained from the simulations are shown in Table IX.

The results shown in Table IX are in accordance with the known fact FSCW machines having a rotationally symmetric configuration have practically zero UMP in absence of rotor eccentricity [24], [25]. This is noted to occur for all the slot-pole combinations in which Z and $2p$ are not relatively prime numbers. Overall, UMP values for conventional and unconventional slot-pole combinations are consistent in their distribution and amplitude.

V. APPLICATION EXAMPLE AND EXPERIMENTAL RESULTS

This Section presents a real case study is which a FSCW with unconventional slot-pole combination is applied to the prototype of a motor-generator for shipboard use, illustrated in Fig. 7.

TABLE IX
SPECIFIC UMP (N/cm^2) FOR VARIOUS SLOT-POLE COMBINATIONS. SHADED CELLS ARE FOR UNCONVENTIONAL COMBINATIONS

Number of slots \ Numbers of poles	2	4	6	8	10	12	14	16	18	20	22	24
3	1.67	4.52										
4	0.01		0.04									
5	0.07	2.64	2.87									
6		0.00		0.00								
7		0.68	3.28	2.08	1.13							
8		0.00	0.00		0.00							
9			0.00	3.96	1.65	0.00						
10			0.00	0.00		0.00	0.00					
11			0.87	0.83	4.62	1.34	0.35					
12				0.00	0.00		0.00	0.00				
13				0.38	0.22	5.28	1.10	1.06	0.44			
14				0.00	0.00	0.00		0.00	0.00			
15					0.00	0.00	5.95	0.98	0.00	0.00		
16					0.00	0.00	0.00		0.00	0.00	0.00	
17					0.31	0.48	0.13	6.59	0.82	0.06	0.24	
18						0.00	0.00	0.00		0.00	0.00	0.00

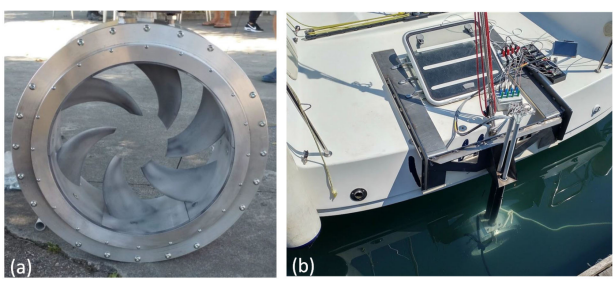

Fig. 7. Prototype motor-generator with a mechanically integrated propeller: (a) before installation; (b) after installation on a boat.

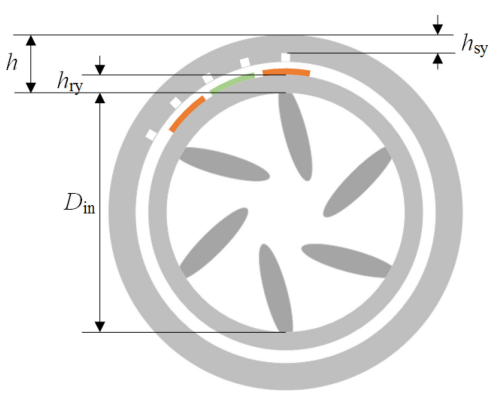

Fig. 8. Schematic machine cross section showing the inner rotor diameter $D_{\rm in}$ as well as stator and rotor yoke heights $h_{\rm sy}$ and $h_{\rm ry}$.

The machine is conceived to operate as an outboard propulsion motor or, when the boat navigates under sail, as a generator to recharge on-board batteries.

A. Dimensional and Functional Requirements

Due to fluid-dynamic reasons, related to propeller optimization, the inner rotor diameter ($D_{\rm in}$ in Fig. 8) is imposed to be equal to 400 mm and the rotor speed to 1000 r/min. Furthermore,

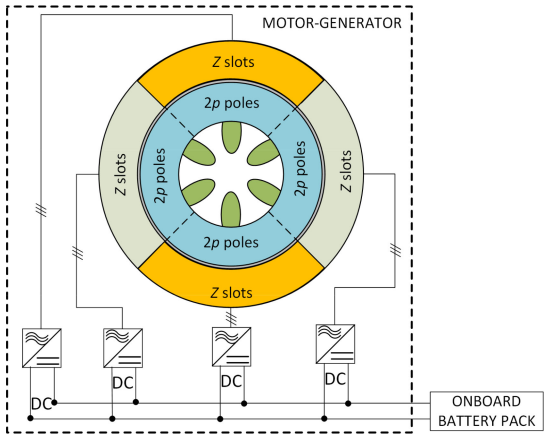

Fig. 9. Functional architecture of the system.

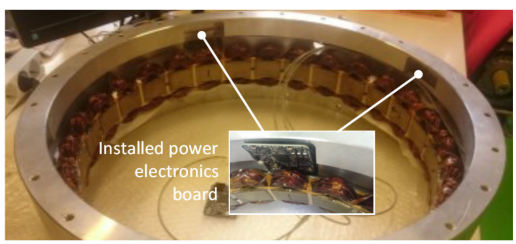

Fig. 10. Machine stator frame and compartments for AC/DC power electronics board installation.

all the radial dimension h of the active parts, including the stator and rotor yoke heights $h_{\rm sy}$ and $h_{\rm ry}$, need be minimized to reduce drag forces during navigation.

From a system-level point of view, the machine is required to consist of four independent three-phase sections, each connected to an AC/DC converter as shown in Fig. 9. The converters are connected to the shipboard DC bus. The segmentation of the system into four modules is aimed at improving fault tolerance (allowing for service continuity at reduced power in case of a faulty module) and is also needed to reduce the size of AC/DC converter power electronics boards, so that they can be mechanically integrated into the machine stator frame (Fig. 10).

Finally, to limit switching and iron core losses within safe limits, the system frequency is constrained not to exceed 200 Hz.

B. Unconventional FSCW Design Choice

The 200 Hz frequency limit combined with the 1000 r/min rated speed leads to a maximum number of poles equal to 24. Furthermore, a very limited room is available (Fig. 10) for stator winding end coils as well as for the connecting cables between the windings and the four converters. This leads to select a dual-layer FSCW (due to its short end coils) and to segment it into four three-phase Z-slot 2-p-pole sections, displaced by 90 degrees apart. In this way, by installing the converters with a 90-degree mutual displacement too (Fig. 10), each three-phase winding section can be located near the relevant converter unit, leading to very short and compact connections.

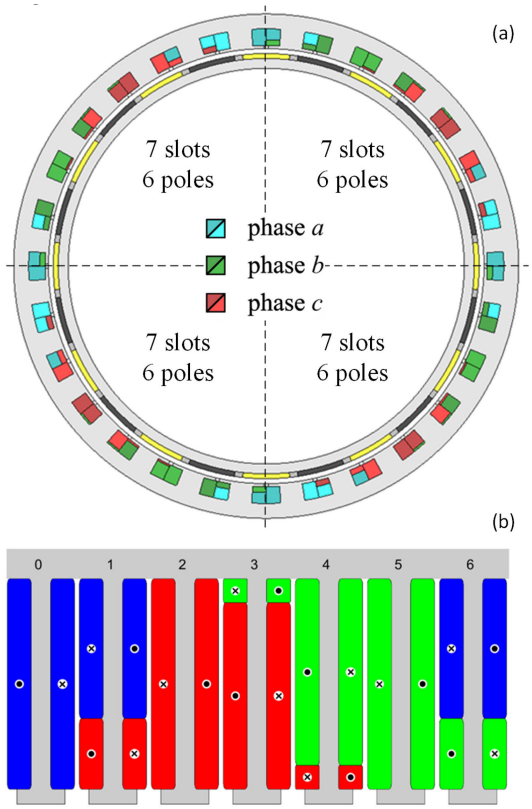

Fig. 11. (a) Motor-generator prototype cross section consisting of four three-phase 7-slot 6-pole sections; (b) FSCW layout for a single section.

TABLE X
STEADY-STATE PEAK-TO-PEAK TORQUE RIPPLE AMPLITUDE AT RATED CONDITIONS WITH SINUSOIDAL STATOR CURRENTS FROM FEA

Slot-pole combination	9 slot 6 poles	8 slot 6 poles	7 slot 6 poles
Peak-to-peak torque ripple in percent of rated torque	14.8%	6.8%	2.7%

Since the overall pole count is constrained not to exceed 24, the number of poles $2p$ of each winding section must be lower than or equal to 6. However, for the fixed inner rotor diameter $D_{\mathrm{in}} = 400$ mm, selecting $p = 1$ or $p = 2$ would call for stator and rotor yoke heights h_{sy} and h_{ry} resulting in excessive radial dimensions h (Fig. 8). Hence, the choice of $p = 3$ appears mandatory. Looking at Table VI, it appears that the only conventional 6-pole FSCW featuring an acceptable winding factor has 9 slots. However, the 9-slot 6-pole configuration suffers from a high torque ripple (Fig. 4) which may cause undesirable vibration and mechanical fatigue over time. At this point, the convenience of using an unconventional slot-pole combination emerges. Good candidates in terms of winding factor (Table VI) would be the 5-slot 6-pole, the 7-slot 6-pole and the 8-slot 6-pole combinations. The first one is discarded due to the relatively high magnet losses (Table VII). The finally selected choice is the 7-slot 6-pole arrangement (Fig. 11) thanks to its high winding factor (Table VI) and low torque ripple (Table X).

Regarding the UMP, it is not a concern because the digital management system is designed so that, in faulty conditions, two diametrically opposite machine sections are disconnected while the other two diametrically opposite sections continue to operate, as in [26]. This guarantees a rotational symmetry (and hence a negligible UMP [24]. [25]) in both healthy and faulty operation, as confirmed by time-stepping FEA simulations.

As it can be seen from Fig. 11(b), the 7-slot 6-pole FSCW, designed with the quadratic programming method described in Section II, is a mixed three- four-layer type [2] including four types of coils, differing by the number of turns. Being $N_{\mathrm{tooth}} = 60$ the maximum number of turns which can be wound around a tooth, the four types of coil respectively comprise the following number of turns: 60, 53, 40, 20 and 7.

The main design data of the machine are summarized in Table XI.

TABLE XI
PROTOTYPE RATINGS AND MAIN DESIGN DATA

Phase voltage	4 × 88 V	Rotor yoke height	10 mm
Phase current	4 × 9 A	Rotor inner radius	200 mm
Speed	1000 rpm	Core length	30 mm
Power factor	1.0	Magnet to pole span ratio	0.85
Number of slots	4 × 7	Stator slot opening width	4 mm
Number of poles	4 × 6	Max. nr. of turns per tooth	60
Stator outer radius	255 mm	Nr. of turns in series per phase	140
Stator bore radius	220 mm	Magnet coercive force	920 kA
Air gap width	5 mm	Magnet relative permeability	1.04
Magnet height	5 mm	Magnet electrical conductivity	0.67 MS/m

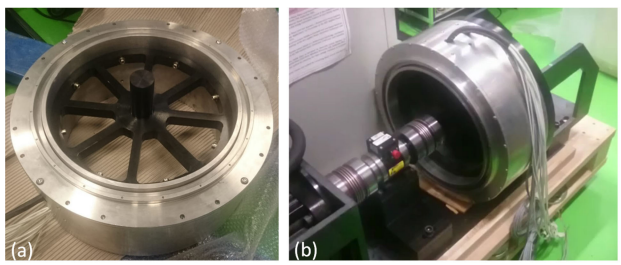

Fig. 12. (a) Machine prototype with blades replaced by a spoked wheel for laboratory testing; (b) coupled prototype on the test bench.

C. Measurements on the Prototype

In the design stage, time-stepping FEA simulations are used to assess the prototype design. As well as for the sample machines considered in Section III, FEA simulations show that the use of an unconventional FSCW does not introduce any kind of unexpected parasitic phenomenon, in both motoring and generating operation modes.

In order to achieve an experimental validation of FEA time-stepping simulations, their results are compared with measurements collected on the prototype during its preliminary laboratory testing (Fig. 12).

The tests have been performed on the machine driven as a generator, with two diametrically opposite sections at open circuit and the other two connected in parallel on an RL load (Fig. 13(a)) or to a diode rectifier feeding a resistor (Fig. 13(b)).

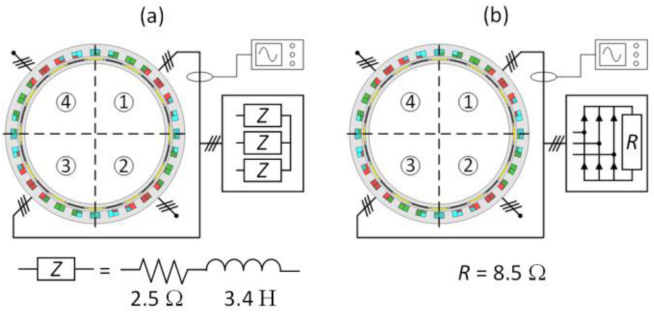

Fig. 13. Prototype test configurations, with Sections II and IV at open circuit and Sections III and IV connected in parallel to (a) an RL load (b) a diode rectifier feeding a resistor.

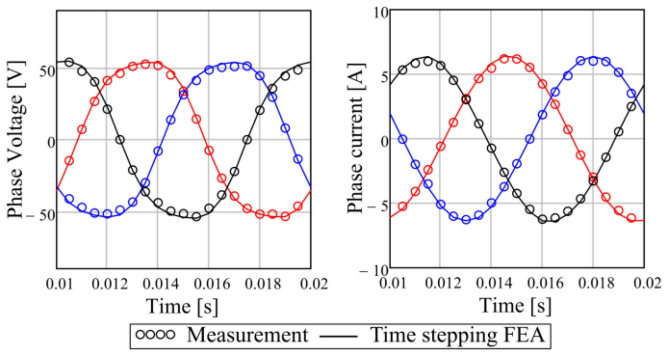

Fig. 14. Phase voltages and currents measured in the test configuration with star-connected RL loads from measurement and time-stepping FEA.

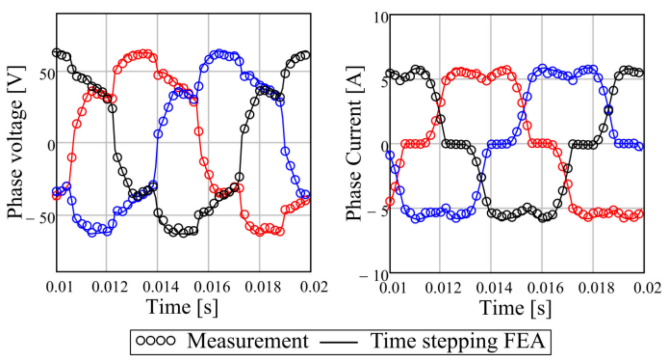

Fig. 15. Phase voltages and currents in the test configuration with a diode rectifier load from measurement and time-stepping FEA.

In the test conducted according to Fig. 13(a), the resistive load is composed of three star-connected RL loads, while in the arrangement depicted in Fig. 13(b) the load consists of a single resistor.

The voltages and currents measured on one phase in the two test arrangements are shown in Fig. 14 and Fig. 15.

It can be seen that the machine, although loaded on only two of its four sectors, exhibits the same balanced symmetrical behaviour that would be expected in case of a conventional FSCW winding. The voltage and current waveforms shown in Fig. 14 and Fig. 15 remain unchanged (they are omitted due to space restrictions) when Sections II and IV of the machine are equally loaded with either the same load as Sections I and III or with a different load.

The satisfactory accordance between measurements and simulation results confirms the reliability of time-stepping FEA as a means for analysing different conventional and unconventional slot-pole combinations in Sections III and IV.

VI. Conclusion

It is a common belief that the design of a symmetrical FSCW is possible only if the number of slots and the number of poles satisfy well-defined algebraic conditions. This paper has shown that perfectly symmetrical FSCWs with slot-pole combinations not respecting such conditions and hence defined unconventional, can be designed if a multi-layer winding layout is adopted. A general algorithm, based on quadratic programming, is presented to synthetize a symmetrical FSCW with an arbitrary number of slots and poles. The method has been illustrated in detail taking the 11-slot 10-pole and the 8-slot 6-pole combinations as case studies. By means of time-stepping FEA, the performance of FSCWs with conventional and unconventional slot-pole combinations have been comparatively assessed in terms of winding factor, rotor eddy-current losses, cogging torque and radial forces without eccentricity. The comparison has shown a substantial consistency between conventional and unconventional slot-pole combinations under all respects, in the sense that unconventional combinations cannot be stated, in general, to behave better or worse than conventional ones. Finally, the possible practical use of an unconventional FSCW has been illustrated by reporting its application to the design of a 28-slot 24-pole permanent magnet machine prototype consisting of four independent 7-slot 6-pole winding sections. The reasons for adopting the unconventional FSCW design have been described. Measurements on the prototype as a driven generator have been reported showing a good accordance with time-stepping FEA simulations and confirming that no unexpected or abnormal effects arise as a consequence of adopting an unconventional FSCW design.

In virtue of its mathematical formulation, the design procedure proposed in this paper for three-phase FSCW's is suitable for an extension to a generic number of phases. Theoretical and experimental results regarding multi-phase and multiple three-phase FSCW's with unconventional slot-pole combinations will be included in forthcoming publications. It will be shown that the adoption of unconventional slot-pole combinations can be particularly useful in multi-phase machines with concentrated winding of small size, where the number of slots needs to be reduced due to geometrical constraints.

Appendix

This Appendix provides a justification of the model (described in Fig. 6) which has been used in Section IV to compare different slot-pole combinations in terms of magnet losses and UMP.

Using the scaling laws reported in Fig. 6, the slot cross-section area changes proportional to $p^2/(Z \times k_{\mathrm{w}})$. Since the number of conductors per slot is maintained constant ($2N_{\mathrm{tooth}} = 200$) as well as the slot fill factor, each conductor cross-section also

grows proportional to $p^2/(Z \times k_w)$. Hence, imposing a phase current equal to $3 \times 4.4\ p^2/(Z \times k_w)$ A results in a constant conductor current density for all slot-pole combinations.

Furthermore, both permanent magnet height and air gap width change proportional to p. Therefore, keeping permanent magnet coercive force constant, the flux density amplitude due to permanent magnets is the same regardless of p. Also the fundamental of the flux density due to the armature reaction does not change. In fact, it is given by:

$$B_{\mathrm{s,fund}} = \frac{M_{\mathrm{fund}}}{g}\mu_0 = \frac{3}{\pi}\frac{k_w}{gp}N_s I_0\,\mu_0, \qquad \text{(A1)}$$

where (17) have been used for M_{fund}; considering that (Fig. 6)

$$I_0 = 3 \times 4.44\,p^2/(Z\ k_w)\mathrm{A},\ g = 0.5p\ \mathrm{mm} \qquad \text{(A2)}$$

and being N_s given by (18), it is clear from (A1) that $B_{\mathrm{s,fund}}$ is independent of both Z and p.

It is therefore demonstrated that the scaling laws given in Fig. 6 guarantee the invariance of the conductor current density, the permanent magnet field and the armature reaction field with respect to Z and p. Of course, the electrical loading A_i, given by [19]:

$$A_i = 6N_s I_0/(2\pi R_s) \qquad \text{(A3)}$$

changes proportional to p/k_w as it can be proved by substituting (A2) and (18) into (A3) and considering that $R_s = 20 \times p$ mm (Fig. 6). However, choosing an electrical loading which grows with the machine size (hence with the pole count according to the model in Fig. 6) is a common and reasonable practice in the design of electric machines [27].

Regarding the UMP, the radial component of the flux density is usually regarded sufficient for its estimation in FSCW machines [28]. Under this assumption, the total force components along two stationary x and y axes having their origin in the machine centre of rotation are given by [29]:

$$F_x(t) = \frac{A_s}{8\mu_0}\mathrm{Re}\left[\bar{b}(t)\right],\ F_y(t) = \frac{A_s}{8\mu_0}\mathrm{Im}\left[\bar{b}(t)\right], \qquad \text{(A4)}$$

where A_s is the stator bore surface area and $\bar{b}(t)$ is a complex function of time which depends only on the radial flux density harmonics produced by the permanent magnets and by the stator currents. It is therefore clear from (A4) that, having chosen a dimensioning law (Fig. 6) which preserves the fundamental flux densities produced by both permanent magnets and stator currents regardless of Z and p, it is possible to compare different slot-pole combinations in terms of UMP performance by considering the maximum force divided by the stator bore surface A_s.

Acknowledgment

The authors wish to gratefully thank the following persons and companies involved in the design, manufacturing, and testing of the prototype described in Section V: Prof. R. Petrella from the University of Udine, Udine, Italy, for power electronics design and prototype laboratory testing; MW FEP, Ronchi dei Legionari, Italy, for power electronics manufacturing; Lampas System, Trieste, Italy, for electric machine manufacturing; and MICAD, Trieste, Italy, for propeller fluid-dynamic design.

References

[1] A. M. El-Refaie, "Fractional-slot concentrated-windings synchronous permanent magnet machines: Opportunities and challenges," *IEEE Trans. Ind. Electron.*, vol. 57, no. 1, pp. 107–121, Jan. 2010.

[2] L. Alberti and N. Bianchi, "Theory and design of fractional-slot multilayer windings," *IEEE Trans. Ind. Appl.*, vol. 49, no. 2, pp. 841–849, Mar./Apr. 2013.

[3] J. F. Gieras, *Electrical Machines: Fundamentals of Electromechanical Energy Conversion*. Boca Raton, FL, USA: CRC Press, 2016, pp. 402–403.

[4] Y. Yokoi, T. Higuchi, and Y. Miyamoto, "General formulation of winding factor for fractional-slot concentrated winding design," *IET Elect. Power Appl.*, vol. 10, no. 4, pp. 231–239, Apr. 2016.

[5] S. E. Skaar, O. Krovel, and R. Nilssen, "Distribution, coil-span and winding factors for PM machines with concentrated windings," in *Proc. 17th Int. Conf. Elect. Mach.*, Chania, Crete Island, Greece, Sep. 2006, Paper 346.

[6] F. Lin, S. Zuo, and X. Wu, "Electromagnetic vibration and noise analysis of permanent magnet synchronous motor with different slot-pole combinations," *IET Elect. Power Appl.*, vol. 10, no. 9, pp. 900–908, Nov. 2016.

[7] S. G. Min and B. Sarlioglu, "Investigation of electromagnetic noise on pole and slot number combinations with possible fractional-slot concentrated windings," in *Proc. IEEE Transp. Elect. Conf. Expo*, Chicago, IL, USA, 2017, pp. 241–246.

[8] M. Valavi, A. Nysveen, R. Nilssen, R. D. Lorenz, and T. Rølvåg, "Influence of pole and slot combinations on magnetic forces and vibration in low-speed PM wind generators," *IEEE Trans. Magn.*, vol. 50, no. 5, pp. 1–11, May 2014.

[9] Z. Q. Zhu and D. Howe, "Influence of design parameters on cogging torque in permanent magnet machines," *IEEE Trans. Energy Convers.*, vol. 15, no. 4, pp. 407–412, Dec. 2000.

[10] L. Zhu, S. Z. Jiang, Z. Q. Zhu, and C. C. Chan, "Analytical methods for minimizing cogging torque in permanent-magnet machines," *IEEE Trans. Magn.*, vol. 45, no. 4, pp. 2023–2031, Apr. 2009.

[11] S. G. Min and B. Sarlioglu, "Analysis and comparative study of flux weakening capability in fractional-slot concentrated windings," *IEEE Trans. Energy Convers.*, vol. 33, no. 3, pp. 1025–1035, Sep. 2018, doi: 10.1109/TEC.2017.2781718.

[12] P. Ponomarev, P. Lindh, and J. Pyrhönen, "Effect of slot-and-pole combination on the leakage inductance and the performance of tooth-coil permanent-magnet synchronous machines," *IEEE Trans. Ind. Electron.*, vol. 60, no. 10, pp. 4310–4317, Oct. 2013.

[13] P. Jalali, S. Taghipour Boroujeni, and J. Khoshtarash, "Expansion of the feasible slot/pole combinations in the fractional slot PM machines by applying three-slot pitch coils," *IEEE Trans. Energy Convers.*, vol. 34, no. 2, pp. 993–999, Jun. 2019.

[14] A. D. Gerlando, R. Perini, and M. Ubaldini, "High pole number, PM synchronous motors with concentrated coil armature winding," in *Proc. Int. Conf. Elect. Mach.*, Krakow, Poland, 2004, Paper 346.

[15] M. V. Cistelecan, F. J. T. E. Ferreira, and M. Popescu, "Three phase tooth-concentrated multiple-layer fractional windings with low space harmonic content," in *Proc. IEEE Energy Convers. Congr. Expo.*, 2010, pp. 1399–1405.

[16] A. Tessarolo, "A quadratic-programming approach to the design optimization of fractional-slot concentrated windings for surface permanent-magnet machines," *IEEE Trans. Energy Convers.*, vol. 33, no. 1, pp. 442–452, Mar. 2018.

[17] N. Tang and I. P. Brown, "Framework and solution techniques for suppressing electric machine winding mmf space harmonics by varying slot distribution and coil turns," *IEEE Trans. Magn.*, vol. 54, no. 5, pp. 1–12, May 2018.

[18] A. Sun, J. Li, R. Qu, and D. Li, "Effect of multilayer windings on rotor losses of interior permanent magnet generator with fractional-slot concentrated-windings," *IEEE Trans. Magn.*, vol. 50, no. 11, pp. 1–4, Nov. 2014.

[19] S. Huang, J. Luo, F. Leonardi, and T. A. Lipo, "A general approach to sizing and power density equations for comparison of electrical machines," *IEEE Trans. Ind. Appl.*, vol. 34, no. 1, pp. 92–97, Jan./Feb. 1998.

[20] F. Giri, *AC Electric Motors Control: Advanced Design Techniques and Applications*. Hoboken, NJ, USA: Wiley, 2013, p. 384.
[21] R. F. Burbidge, "A rapid method of analysing the m.m.f. wave of a single or polyphase winding," *Proc. IEE C, Monographs*, vol. 105, no. 7, pp. 307–311, Mar. 1958.
[22] N. Bianchi and E. Fornasiero, "Impact of MMF space harmonic on rotor losses in fractional-slot permanent-magnet machines," *IEEE Trans. Energy Convers.*, vol. 24, no. 2, pp. 323–328, Jun. 2009.
[23] S. Stipetic, D. Zarko, and M. Popescu, "Ultra-fast axial and radial scaling of synchronous permanent magnet machines," *IET Elect. Power Appl.*, vol. 10, no. 7, pp. 658–666, 2016.
[24] Z. Q. Zhu, D. Ishak, D. Howe, and J. Chen, "Unbalanced magnetic forces in permanent-magnet brushless machines with diametrically asymmetric phase windings," *IEEE Trans. Ind. Appl.*, vol. 43, no. 6, pp. 1544–1553, Nov./Dec. 2007.
[25] G. H. Jang, J. W. Yoon, N. Y. Park, and S. M. Jang, "Torque and unbalanced magnetic force in a rotational unsymmetric brushless DC motors," *IEEE Trans. Magn.*, vol. 32, no. 5, pp. 5157–5159, Sep. 1996.
[26] A. Tessarolo, F. Luise, S. Pieri, A. Benedetti, M. Bortolozzi, and M. De Martin, "Design for manufacturability of an off-shore direct-drive wind generator: An insight into additional loss prediction and mitigation," *IEEE Trans. Ind. Appl.*, vol. 53, no. 5, pp. 4831–4842, Sep./Oct. 2017.
[27] J. Pyrhonen, T. Jokinen, and V. Hrabovcova, *Design of Rotating Electrical Machines*. Hoboken, NJ, USA: Wiley, 2008, p. 293.
[28] Z. Q. Zhu, Z. P. Xia, L. J. Wu, and G. W. Jewell, "Analytical modeling and finite-element computation of radial vibration force in fractional-slot permanent-magnet brushless machines," *IEEE Trans. Ind. Appl.*, vol. 46, no. 5, pp. 1908–1918, Sep./Oct. 2010.
[29] D. G. Dorrell, M. Popescu, C. Cossar, and D. Ionel, "Unbalanced magnetic pull in fractional-slot brushless PM motors," in *Proc. IEEE Ind. Appl. Soc. Annu. Meeting*, Edmonton, AB, Canada, 2008, pp. 1–8.

Alberto Tessarolo received the Laurea degree in electrical engineering from the University of Trieste, Italy, in 2000, and the Ph.D. degree in electrical engineering from the University of Padova, Padova, Italy, 2011. Before joining the university, he worked in the design and development of large innovative motors, generators, and drives. Since 2006, he has been with the Engineering and Architecture Department, University of Trieste, where he teaches the courses of electric machine fundamentals and electric machine design. He leads several funded research projects in cooperation with industrial companies for the study and development of innovative electric motors, generators, and drives. He authored more than 150 international papers in the area of electrical machines and drives. He has been an Associated Editor for the IEEE TRANSACTIONS ON ENERGY CONVERSION, IEEE TRANSACTIONS ON INDUSTRY APPLICATIONS, and *IET Electric Power Applications*. He is currently the Editor-in-Chief for the IEEE TRANSACTIONS ON ENERGY CONVERSION. He is a member of the Rotating Machinery Technical Committee (TC2) of the International Electrotechnical Commission (IEC) and supports the definition of IEC standards on inverter-fed electric motors. He is also a member of the IEEE Power and Energy Society Electric Machinery Committee, the IEEE Industry Applications Society Electric Machines Committee, and the IEEE Industrial Electronics Society Electric Machines Technical Committee.

Cesare Ciriani received the Laurea degree in electrical engineering from the University of Trieste, Trieste, Italy, in 2017. He is currently working toward the Ph.D. degree in electrical engineering with the University of Trieste. His research interests include modeling, analysis, and design optimization of electric machines.

Mauro Bortolozzi received the Laurea and Ph.D. degrees in electrical engineering from the University of Trieste, Trieste, Italy, in 2012 and 2016, respectively. From 2016 to 2019, he was a Research Fellow with the University of Trieste, working in the field of electric machine design and optimization. Since 2019, he has been with Rete Ferroviaria Italiana, Trieste, where he deals with the design and management of the Italian railway electrical infrastructures. He is a Registered Professional Engineer in Italy and a member of the Italian Association of Electrical, Electronics, Automation, Information, and Communication Technology (AEIT).

Mario Mezzarobba received the Laurea degree in electrical engineering from the University of Trieste, Trieste, Italy, in 2009, and the Ph.D. degree in electrical engineering from the University of Padova, Padova, Italy, in 2014. Since 2014, he has been a Research Fellow with the University of Trieste and has actively taken part in several research projects for the dimensioning, design, prototyping, and testing of electromechanical actuators, components, and systems. His main research interests are in the field of induction motor, permanent-magnet machine, and electromagnetic stirring analysis, design, and optimization.

Nicola Barbini received the Laurea degree from the University of Trieste, Trieste, Italy, in 2012. He is currently working toward the Ph.D. degree in electrical engineering from the University of Trieste. His research focuses on the modeling and analysis of electric machines and power transformers.